Fluid Motion and Heat Transfer in an ASTM-E659 Apparatus

Branson Davis[a,*], Charline Fouchier[a,b] and Joseph E. Shepherd[a]

[a] *California Institute for Technology, Pasadena, USA*
[b] *von Karman Institute for Fluid Dynamics, Sint-Genesius-Rode, Belgium*

ARTICLE INFO

Keywords:
Thermal Ignition
Standardized Tests
Heat Transfer
Fluid Mechanics
Safety

ABSTRACT

In this study, experimental measurements and three-dimensional numerical simulations were used to characterize the non-reactive gas motion and mixing inside the flask of our laboratories' Autoignition Temperature (AIT) facility based on the ASTM-E659 standard. Downward plumes of cool air enter through the open top of the flask, through the neck, and into the spherical vessel. This creates a single dominant toroidal vortex that transports fluid upwards along the walls and downward along the center line. Increasing the height of the flask holder caused the average temperature to increase and the magnitude/frequency of fluctuations to decrease. Studies of fuel-air mixing of ethene (C_2H_4), n-hexane (nC_6H_{14}), and n-dodecane ($nC_{12}H_{26}$) found that the lighter fuels more readily diffuse into air whereas the heavier fuels are more strongly influenced by buoyancy effects and take longer to mix. Further, in some cases the mixing time will be comparable to the time to ignition and long ignition times may result in significant quantities of fuel molecules escaping from the open top of the flask.

1. Introduction

The minimum autoignition temperature (AIT) of a fuel in hot air is used to evaluate the flammability and fire hazards of combustible gases and liquids. Early theoretical work by Semenov (1928) and Frank-Kamenetskii (1939) treated autoignition as a self-heating phenomenon where thermal feedback between exothermic chemical reaction competes with heat transfer to create critical conditions for ignition. The earliest models either considered stirred batch reactors (Semenov) or conduction in a stationary material (Frank-Kamenetskii) where the heat transfer was modeled by engineering correlations at the boundaries. Application and extension of these approaches has created a substantial body of work with stimulating mathematical analyses (Zeldovich, Barenblatt, Librovich and Makhviladze, 1985) and applications to industrial safety (Hattwig and Steen, 2004; Babrauskas, 2003; Bowes, 1984).

The earliest experimental tests of the autoignition theory used decomposition of highly reactive gases (azides and peroxides) in heated glass flasks (Rice, Allen and Campbell (1935)). Although the results were initially largely in accord with the Semenov model, Rice and Campbell (1939) made an observation in replies to comments on their paper that: "Possibly convection is important at high pressures. Our results on the heat loss constant indicate that this may the case, but more work, both theoretical and experimental needs to be done. My impression is that thermal conduction is not enough to account for the loss of heat even at low pressures but this view may need correction."

Subsequent studies have focused on the potential role of convection during filling and ignition, emphasizing the localized temperature variation associated with the onset of exothermic reaction. Experimental studies by Tyler (1966) and later by Ashmore, Tyler and Wesley (1967) examined the effect exothermic chemical reaction had on heat transfer in closed spherical vessels. For slow reaction rates, the resultant local temperature rise was low and exhibited good agreement with the theoretical results from Frank-Kamenetskii. However, for faster reaction rates, the larger increase in local temperature caused significant convection to occur that caused an asymmetry of the vertical temperature profile and deviation from the theoretical model. Tyler and Tuck (1967) demonstrated experimentally using inert gases (H_2, N_2, CO_2) that temperature differences as small as 5 K between the gas and walls could induce significant natural convection in 280 and 1100 cm^3 spheres. Tyler and Tuck proposed that the onset of natural convection could be correlated with using a Rayleigh number of 600, consistent with the observations of temperature profiles observed in the reacting tests (Tyler, 1966; Ashmore et al., 1967).

Numerical simulations (Jones, 1974; Kee, Landram and Miles, 1975; Silakova, Smetanyuk and Pasman, 2006; Campbell, Cardoso and Hayhurst, 2007) demonstrate that for modest values of the Rayleigh number (≤ 600), natural convection in a reacting flow results in a a toroidal vortex within a closed flask. Gas rises through through the center and falls along the outer surfaces of a cylinder or spherical container. The implications of heat-release generated convection on autoignition was explored through numerical simulation by Silakova et al. (2006); Liu, Campbell, Hayhurst and Cardoso (2010); Liñán, Moreno-Boza, Iglesias, Sánchez and Williams (2016); Sánchez, Iglesias, Moreno-Boza, Liñán and Williams (2016); Iglesias, Moreno-Boza, Sánchez, Liñán and Williams (2017) and most recently by Melguizo-Gavilanes, Boettcher, Mével and Shepherd (2019).

Quite separately from the theory of self-ignition and laboratory experiments, the development of standardized tests for autoignition (Setchkin, 1954; Zabetakis, Furno and Jones, 1954) was driven by the need to regulate the shipping and handling of combustible liquids to minimize fire

---

[*] Corresponding author

bdavis@caltech.edu (B. Davis)
ORCID(s): 0000-0002-5288-7913 (B. Davis); 0000-0002-6910-9982 (C. Fouchier); 0000-0003-3181-9310 (J.E. Shepherd)

hazards. These initial studies created methodology and apparatus that have evolved into the modern day ASTM-E659 (2005) standard in North America and the comparable international standard ISO/IEC 80079-20-1 (2017). During testing, a small quantity of liquid fuel is injected into a glass flask containing hot air at atmospheric pressure. The AIT is the minimum temperature for which ignition is observed within a limited time period in a series of trials varying the fuel amount and flask temperature following the procedure set out in the standard. The US standard uses a 500 mL round bottom flask while the European standards (ISO/IEC 80079-20-1, 2017) use a smaller, 200 mL, flat bottom (Erlenmeyer) flask. Both the tests immerse the flask within a temperature-controlled oven and inject fuel through the open mouth of the flask. The top of flask remains open during testing to enable visualization of light emission associated with ignition.

The ASTM-E659 standard and the related ISO standards such as EN 14522 and DIN 51794 (ISO/IEC 80079-20-1, 2017) have been extensively used to characterize AITs for various liquid fuels. The reported AITs are tabulated in combustion safety databases, such as the Chemical Hazard Response Information System (CHRIS) and CHEMSAFE (USCG, 1999; Zakel, Brandes and Schröder, 2019). Recent experimental results of Martin and Shepherd (2021) emphasized that a wide range of ignition behaviors can occur, which could be categorized into at least four distinct modes. Measured AITs are also found (Lüth, Brandes and Stolz, 2014; Johnson and Mashuga, 2023) to be sensitive to the specifics of the measurement technique, with variability often exceeding the precision of published data. To better understand and reduce variability in test results, our laboratory is working on modeling and improvements in test methodology of the E659 test.

In addition to the convective effects caused by exothermic chemical reaction in closed spherical vessels, we have noticed that there are significant non-reactive convective effects due to the design and operation of industrial tests like E659. Recent experiments with our own ASTM-E659 apparatus indicate that the transient heat transfer and fluid motion inside the flask that exists as a consequence of the unsealed top and fuel injection are important to consider in creating realistic models of industrial autoignition tests. These effects have not been considered in previous numerical and analytical studies that assume closed vessels with initially homogeneous mixtures.

In order to investigate the effects of actual geometry and boundary conditions of a representative standardized test, we used numerical modeling of three-dimensional unsteady flow within the actual geometry of our E659 apparatus. The motion of the air above flask, inside the neck, and within the flask were modeled using temperature variations along the flask surface representative of measured values. Although we only describe non-reactive results in the present report, these results have important implications for the initial conditions of reactive simulations which will be presented in a subsequent report from our laboratory.

The focus of this study is to investigate the effect various experimental setups conforming to the ASTM-E659 standards could have on the flow field inside the flask and temperature measurements used to report AITs. The temperature profile along the axis of symmetry inside the flask was characterized experimentally and compared with three-dimensional, unsteady numerical simulations. The influence of the mixing zone between outside air and the flask interior was identified as a key factor in determining the mean and fluctuating temperature profile in the flask. Numerical simulations of fuel-air mixing studies were conducted to characterize the transient mixing process that takes place after fuel is introduced into the flask.

2. Experimental Methods

For our study, we adapted the experimental setup used by Martin and Shepherd (2021) for the characterization of the AITs for Jet A and surrogate jet fuels. This apparatus was constructed following the ASTM-E659 (2005) standard. Figure 1 shows a picture and a cross-section drawing of the setup.

The apparatus is composed of a Mellen CV12 crucible furnace with a 133 mm diameter and 200 mm deep cylindrical volume, which controllably heats a 500 mL round bottom, borosilicate flask up to 1250 °C with a PID controller (Love Controls series 16B) system accurate to 1 °C. The flask is suspended in the furnace by a ceramic holder molded from silica-based Cotronics Rescor 750. The flask and ceramic holder are covered by aluminum foil to reflect the radiation inside the flask and reduce heat loss.

The temperature of the flask surface is measured with three 34 gauge, type K thermocouples inside a mineral-insulated metal sheath, set at positions T_1, T_2, and T_3 (see Figure 1). The thermocouple conventionally used to measure the air temperature, T_4, in ignition experiments was removed and replaced with a 36 gauge, type K thermocouple attached to a Velmex slide (NEMA 17, 155 mm travel) capable of precise vertical resolution. This allowed temperature measurements to be taken at various heights within the apparatus. The temperature variation is recorded with a NI 9213 16-channel, 24-bit, 75 Hz thermocouple data acquisition module from National Instruments, connected to a cDAQ-9171 CompactDAQ Chassis. We sampled each height for 120 s and waited an additional 120 s between measurements to allow unsteadiness effects caused by the movement of the internal thermocouple to dampen.

3. Numerical Methods

The transient, three-dimensional fluid motion, heat transfer, and mixing were numerically simulated directly by solving the Navier-Stokes equations of a multi-component ideal gas mixture. The equations of motion Eqn. (1)-(4), boundary and initial conditions were solved in OpenFOAM using the *buoyantReactingFoam* solver with reactions disabled. We only considered non-reacting flow and did not attempt to

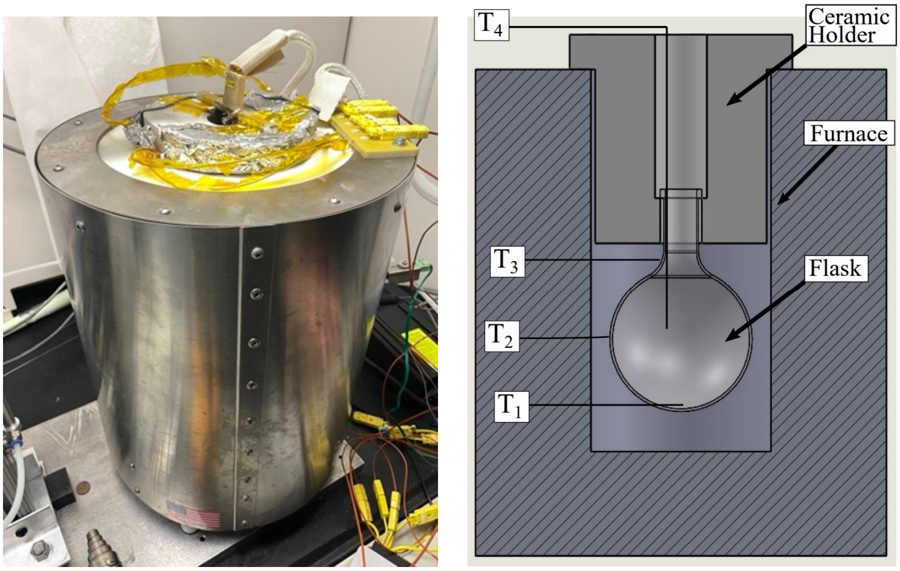

Figure 1: Experimental apparatus

model chemical reactions or the actual autoignition process in this study.

3.1. Geometric Model and Meshing

The flask and ceramic holder of the ASTM setup shown in Figure 1 were carefully measured and modeled in Solidworks to provide a suitable framework for simulation. The interior geometry was then meshed in three dimensions using the OpenFOAM tool, snappyHexMesh, prioritizing uniform hexahedral cells. A grid-independent solution, as determined from a statistical analysis of the unsteady flow, could be achieved for a grid of 6 million cells resulting in cell sizes of approximately 600 μm. In addition to modeling the flask and ceramic holder, a rectangular region above the flask (not shown in Figure 2) with open boundaries was included to model the exchange of gas between the flask and the surrounding atmosphere.

3.2. Governing Equations

The governing equations we simulated were the variable-density Navier-Stokes equations for a Newtonian fluid with temperature-dependent transport properties and buoyancy forces in the momentum equation.

$$\frac{\partial \rho}{\partial t} + \nabla \cdot (\rho \mathbf{u}) = 0\,, \tag{1}$$

$$\frac{\partial}{\partial t}(\rho \mathbf{u}) + \nabla \cdot (\rho \mathbf{u}\mathbf{u} + p\mathbf{I}) = \nabla \cdot \tau + \rho \mathbf{g}\,, \tag{2}$$

$$\frac{\partial}{\partial t}(\rho Y_i) + \nabla \cdot (\rho Y_i \mathbf{u}) = -\nabla \cdot (\rho Y_i \mathbf{V}_i) \quad i = 1, 2, \dots, K\,, \tag{3}$$

$$c_P \frac{\partial}{\partial t}(\rho T) + c_P \nabla \cdot (\rho \mathbf{u} T) = -\nabla \cdot (\lambda \nabla T) - \rho \nabla T \cdot \sum_{i=1}^{K} c_{P,i} Y_i \mathbf{V}_i\,, \tag{4}$$

where t is time, ρ is the mixture density, p is the pressure, u is the velocity, g is the acceleration due to gravity, T is the temperature, c_P is the specific heat at constant pressure, λ is the mixture thermal conductivity, Y is the mass fraction, $\mathbf{V}$ is the correction diffusion velocity, and τ is the viscous stress tensor written as:

$$\tau = \mu(\nabla \mathbf{u} + (\nabla \mathbf{u})^T) - \frac{2}{3}\mu(\nabla \cdot \mathbf{u})\mathbf{I} \tag{5}$$

where $\mathbf{I}$ is the identity matrix. The subscript, i, indicates the individual species, and K is the total number of species. For simulations in air, the species conservation equation and mass diffusion term in the energy equation were omitted. The ideal gas equation of state was used to calculate the density of the mixture.

The diffusion velocities are calculated according to Chapman and Cowling (1990) using Fick's law, including a contribution by thermodiffusion (Soret effect) as:

$$\mathbf{V_i} = -\frac{D_i}{Y_i}\nabla Y_i - \frac{D_i \Theta_i}{X_i}\frac{1}{T}\nabla T \tag{6}$$

where X_i is the mole fraction, and Θ_i is the thermodiffusion ratio of species i. The individual-species mixture-averaged diffusion coefficients, D_i, are calculated according to Curtiss and Hirschfelder (1949) as:

$$D_i = \frac{1 - Y_i}{\sum_{j \neq i}^{N} \frac{X_i}{\Gamma_{ji}}} \tag{7}$$

where Γ_{ji} are the binary diffusion coefficients. To ensure the conservation of mass, a correction diffusion velocity is applied to $\mathbf{V}_i$ in Eqs (3) and (4) as described by Coffee and Heimerl (1981) as:

$$\mathbf{V}_i^C = \mathbf{V}_i + \mathbf{V}_C\,. \tag{8}$$

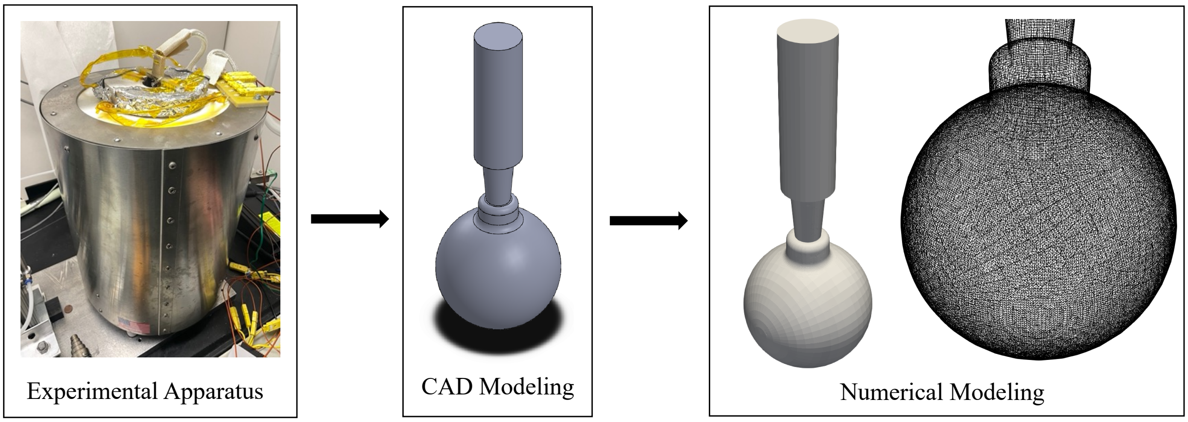

Figure 2: Numerical Modeling of the ASTM apparatus

3.3. Initial and Boundary Conditions

Figure 3 shows the temperature boundary condition on the flask and holder as a function of height. A piece-wise linear profile in height z was imposed on the surface of the flask and was assumed constant in the holder section due to the large ceramic mass being held inside the furnace. These temperatures correspond to experimentally measured flask surface temperatures $T_1 = 521$ K, $T_2 = 527$ K, and $T_3 = 518$ K. A no-slip condition was imposed on the walls.

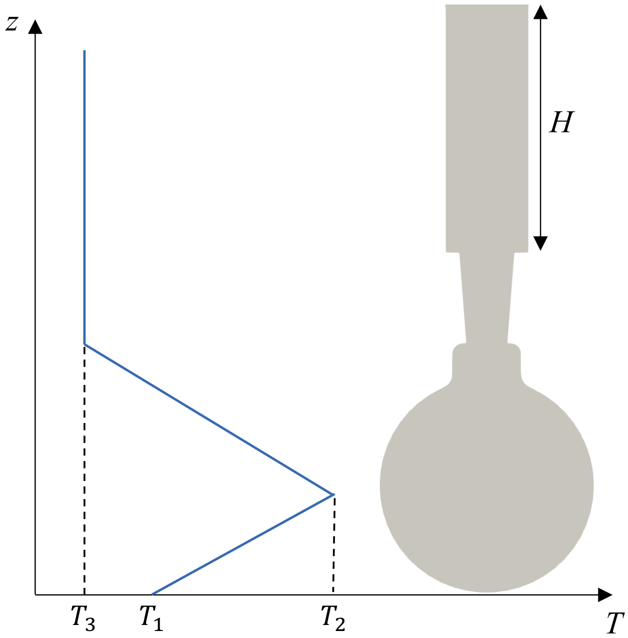

Figure 3: Height-varying temperature boundary condition

The simulations were initiated from rest at room temperature and continued until the temporal flow field became statistically stationary. Flow characterization and mixing simulations used this resultant flow field as an initial condition.

Table 1
Geometric holder configurations

Case	Holder Height H (mm)
A	57.15
B	114.3
C	228.6

3.4. Test Conditions

The initial and boundary conditions were used to characterize a dry air flow field for various height ceramic holder pieces within the specs of the ASTM-E659 standard, which are summarized in Table 1. The inner diameter for all holders was 38.1 mm.

Case B corresponds to the dimension of the ceramic holders used in our laboratory and was used to numerically examine fuel mixing within the flask for gaseous ethene (C_2H_4), n-hexane (nC_6H_{14}), and n-dodecane ($nC_{12}H_{26}$). The ASTM-E659 standard with an open flask is intended for liquid or solid substances. Ethene was examined in order to investigate the effect of lighter, more diffusive fuels on the mixing process and efflux. Although the ASTM standard uses a closed flask for gas testing, the ISO/IEC 80079-20-1 (2017) international standard allows the testing of gas in an open flask similar to the ASTM liquid apparatus. The syringe injection process was not simulated, but instead, a 15 mm ball of fuel was initialized into a fully established flow field at the internal flask temperature. The resulting evolution of the composition (without reaction) was characterized as a function of time and space.

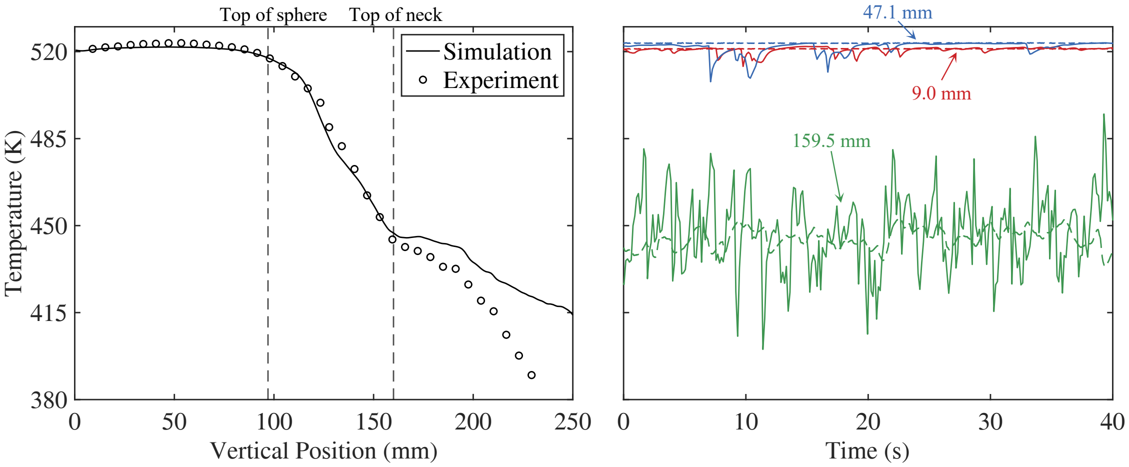

Figure 4: (Left) Average temperature along the vertical center line of the flask, comparing simulation and experiment. (Right) Comparison of temperature fluctuations at selected heights between the simulation (solid lines, –) and experiment (dashed lines, - -)

4. Results and discussion

4.1. Experimental Validation

To validate the numerical model, temperature measurements were digitally recorded and temporally averaged for a series of points on the vertical center line of the experimental apparatus and compared with values from the equivalent numerical simulation of case B. The position 0 mm corresponds to the bottom of the flask. Figure 4 (left) compares the average temperature between the experiment and the simulation. The vertical dashed lines indicate the top of the lower, spherical part of the flask (98 mm) and the upper neck of the flask (159 mm). A variation of 4 K was seen across the lower portion of the flask. Through the neck, a more significant 75 K temperature variation was seen due to the mixing region at the exit of the flask and within the ceramic holder. Above the flask, the temperature decreases with increasing height, approaching the value of the cold ambient air above the setup.

Comparing the average temperature between the simulation and the experiment within the lower part of the flask, the maximum deviation was only 1.5 K for any measured position. However, larger deviations in the temperature profile inside the ceramic holder can be observed. The surface temperature profile within the ceramic holder was not measured and was assumed to be spatially uniform in the simulation. This assumption is likely the source of discrepancy between simulation and experiment in this region.

Computed and observed temporal temperature fluctuations are shown in Figure 4 (right) at heights of 9, 47.1, and 159.5 mm along the flask center line. These heights correspond to the bottom, middle, and region immediately above the top of the flask. In the simulations, fluctuations up to 5 K are observed at the bottom of the flask and up to 12 K at the center of the flask. Immediately above the top of the flask, the flow is very unsteady. Fluctuations up to 80 K are observed with durations of approximately 0.1 s. The experimentally measured fluctuations for all heights are significantly less than those simulated, only 20 K at most above the flask in the ceramic holder. This difference is due to the slow response time of the thermocouple used for the measurements, estimated to have a characteristic step response time of $\tau = 1$ s to reach 67% of the final value. This is at least an order of magnitude slower than the fluctuations observed in the simulations and accounts for the observed differences.

4.2. Effects of holder height

The ASTM standard allows users flexibility in the construction of the apparatus and in particular, the dimensions of the ceramic holder and the location of the flask within the furnace. We examined the influence of the three insulating holder heights shown in Table 1 on the fluid motion. The motion was simulated for 50 seconds after stationary statistics were achieved that were independent of start-up behavior. Figure 5 plots on a vertical cross-section through the center line the average temperature field and projected (surface) streamlines. For all three cases, a toroidal vortex is observed within the bottom of the flask where air sinks through the center of the flask and rises along the walls. The flow is in the unsteady but laminar regime with an estimated Reynolds number (based on flask diameter and maximum center line gas velocity) of $Re \approx 120$. Flow is driven by both the small surface temperature distribution on the flask and, more importantly, the flow of colder, more dense air penetrating down the ceramic holder through the center of the flask and an upward counterflow of hot air circulating from the bottom portion of the flask upward along the hot walls. Circulation cells commonly observed in natural convection flows within nonuniformly heated slots or cavities are observed above the flask within the ceramic holder. As the holder height is increased, the number of cells increases, from 2 to 10.

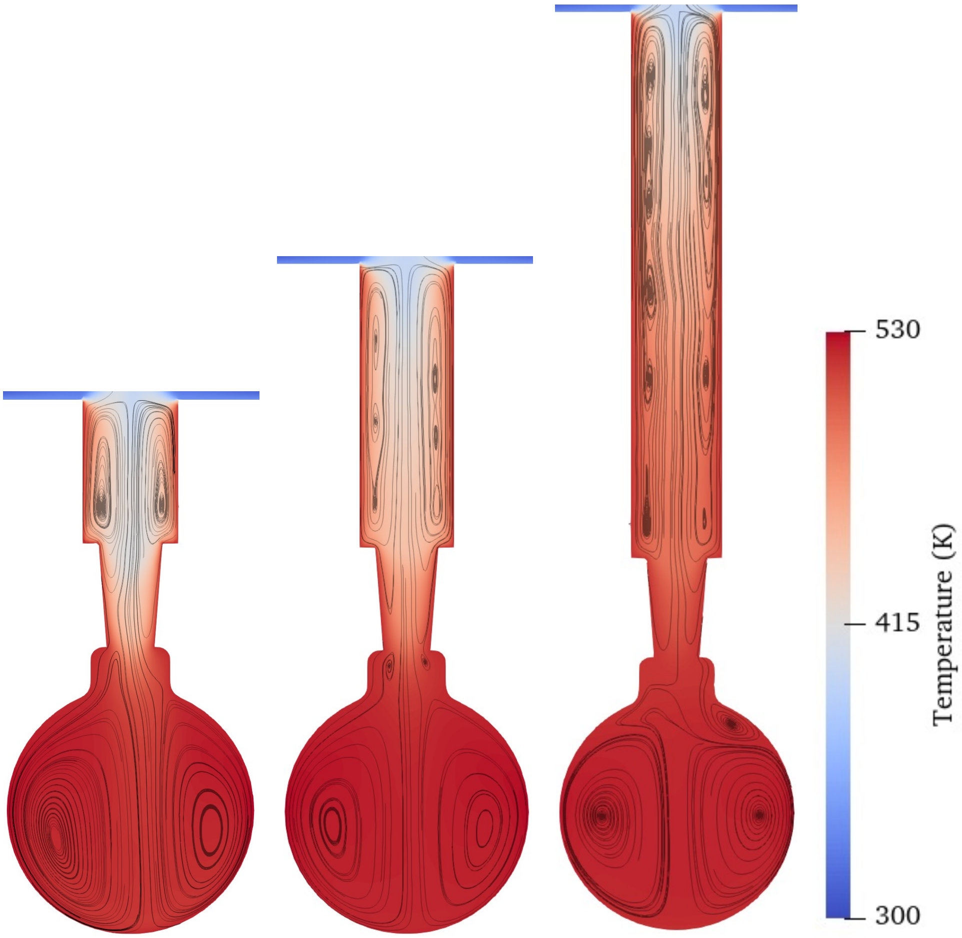

Figure 5: Average temperature field and surface streamlines along a vertical cross-section of the domain for the three holder heights

The averaged flows are approximately axisymmetric but evidence of the three-dimensional motion and symmetry-breaking can be observed in the surface streamline patterns.

The results from Figure 5 show the existence of an unsteady toroidal vortex which is evidence of convection independent from any chemical reaction. In contrast to vortical motion observed in self-heating tests and computations that are discussed in the Introduction, the vortex rotates in the opposite direction and is a direct consequence of nonreactive flow, the intrusion of cold air downward through the open mouth of the flask. The sinking cold air mixes with the hot air in the entrance to the flask, penetrates on the center line into the main volume and creates an average vortical motion within the flask, with hot air rising along the side walls.

Examining the average temperature field, an unstable vertical stratification is apparent within the holder, with temperature decreasing with increasing height, as shown in Figure 6 (left). Modest variations in temperature can be observed within the round portion of the flask, case A was on average 7 K lower than case C. The temperature variations within the neck of the flask decrease with the increasing height of the ceramic holder. This is due to the increased mixing and longer residence time of the cold ambient gas as it plunges down through the longer holders into the flask. The cold air above the furnace has to travel further to reach the flask in case C compared to case A. The average downward velocity, Figure 6 (right), is lower in case C than in case A leading to a longer mixing time and greater heat transfer. Therefore, larger average temperatures are observed as the holder height increases. Transverse velocities along the center line (not shown) are two orders of magnitude smaller than the vertical component.

While averages can be informative about the large-scale features of the flow, temperature fluctuations[1] are important for unsteady reactive flow problems since reaction rates strongly depend on temperature. Table 2 gives the temporal temperature statistics in the center of the flask. This location is consistent with the nominal location of thermocouple T_4, used by the ASTM-E659 standard to monitor and characterize the temperature within the flask during ignition experiments. Case A had the largest temperature standard deviation (8 K) and largest absolute fluctuation size (38 K), while case C had the smallest standard deviation (0.9 K) and

---

[1] Correlations between temperature and composition and conditional averages of reaction rates are also important but we only examined non-reacting aspects of the flow in this study.

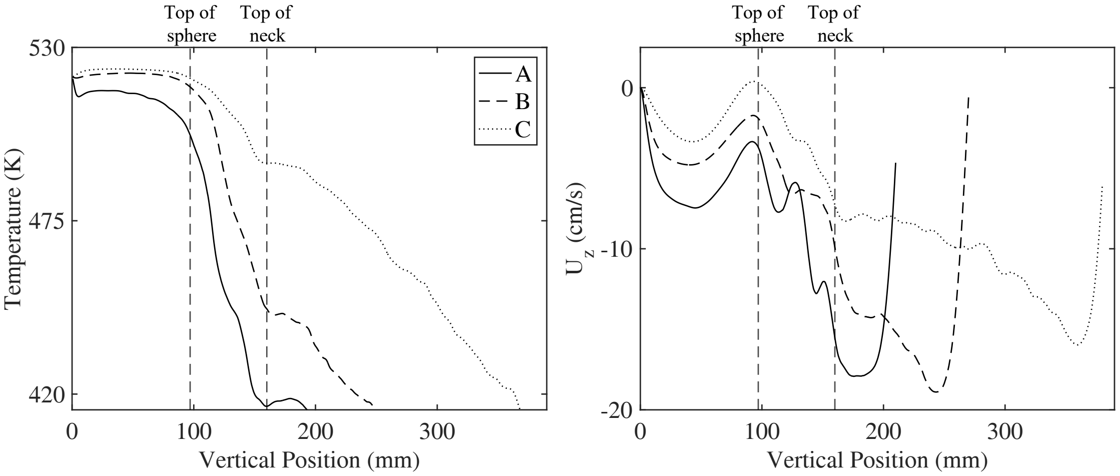

Figure 6: (Left) Average temperature profile and (Right) Average vertical velocity along the vertical center line for the three holder heights

Table 2
Statistical analysis of temperature at the center of the flask for the three holder heights

Case	T_{avg} (K)	T_{std} (K)	T_{min} (K)	T_{max} (K)
A	515.6	8.00	477.2	522.1
B	520.6	3.30	494.3	523.6
C	522.8	0.90	519.7	524.1

absolute fluctuation size (3 K). This is expected since the residence times of downward moving cold air are smaller in the shorter flask holder as compared to the taller holders.

The temporal average temperature was computed for all cells within the spherical portion of the flask. A histogram was obtained by binning the average temperature field. This is directly related to the probability distribution as the computational volumes are essentially identical in size and uniformly distributed. Figure 7 plots the distributions for the three holder heights. The location of the temperature at the center of the flask, T_4, is indicated with vertical lines. For the shortest holder, case A, the distribution is broadest, spanning 15 K, whereas cases B and C are narrower, spanning 9 and 8 K, respectively. These trends are consistent with the fluctuations reported in Table 2. With decreasing holder height, the flow fields become less steady and more cold air enters the flask, broadening the temperature probability distribution. For all holders, T_4 is on the left tail of their respective distributions with values of T_4 up to 5 K less than the median temperature. The implications for the reported AIT are discussed in Section 5.

4.3. Fuel Mixing

During an ignition experiment, fuel is injected from a syringe through a thin needle into the flask. Depending on the temperature, ignition can occur at a range of times following injection and with different extents of mixing depending on the fuel density and diffusivity. Understanding how the fuel distribution evolves within the flask following injection is also relevant to explaining the various modes of ignition that have been observed (Martin and Shepherd, 2021).

To study the effect of mixing, a ball of fuel in its gaseous phase was initialized near the bottom of the flask in an established dry air flow field. The temperature of the fuel sphere was set to be equal to the local air temperature at the time of injection. An initial fuel temperature closer to room temperature (300 K) was also examined and mixing behavior for these cases are briefly discussed. All presented results besides the blue curves in Figure 10 are for the flask ambient temperature fuel initialization cases. We acknowledge that a more complicated situation exists for liquid fuels, with droplets and two-phase mixtures emerging from the needle. The flow momentum, droplet vaporization, impact on the flask surface, and droplet dynamics, including the Leidenfrost effect, will influence the mixing behavior. Chemical reactions will also begin to take place concurrent with the mixing process. We have drastically simplified the problem to enable a preliminary analysis.

The evolution of fuel concentration over time was computed for three fuels of very different sizes and molecular weights. Figures 8 and 9 plot the mole fractions of C_2H_4 and nC_6H_{14} on a vertical cross-section through the center of the flask over time. The color bar is updated at every instance in time so that the mixing characteristics can be visualized. For the C_2H_4 case, the fuel initially rises slightly before being fully mixed in the flask within 30 seconds. The nC_6H_{14} and $nC_{12}H_{26}$ (not shown) cases mix very differently than C_2H_4. For the heavy molecules, the fuel initially sinks to the bottom of the flask before diffusing upwards and becoming fully mixed over a much longer period, 100-200 s.

The effect of varying the fuel molecular weight and temperature can be characterized by the density of the fuel

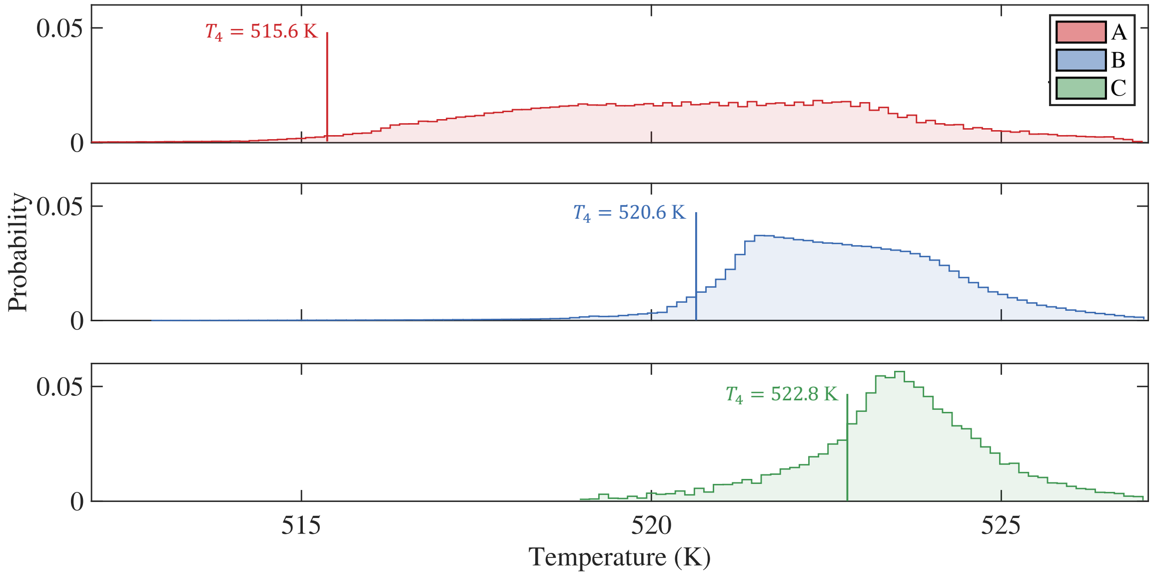

Figure 7: Flask average temperature probability distributions for the three holder configurations. Flask center temperatures, T_4, are also indicated.

sphere, ρ_F, the Froude number based on peak center line speed U, flask diameter d, and density normalized density difference $\Delta\rho/\rho_F = (\rho_F - \rho)/\rho_F$ between the fuel volume and surrounding air

$$Fr = \frac{U}{\sqrt{gd|\Delta\rho|/\rho_F}} \cdot \mathrm{sgn}(\Delta\rho_F)\,,$$

and the Schmidt number based on the mixture viscosity μ and fuel diffusivity D_F in the surrounding fuel-air mixture

$$Sc = \frac{\mu}{\rho D_F}\,.$$

Representative values for each fuel are shown in Table 3. Because all the cases were initialized at the same temperature and pressure, the initial density of the ethene sphere is slightly smaller than the ambient air density (0.69 kg·m^{-3}) and the initial density of the n-hexane and n-dodecane spheres are larger than ambient. As a consequence, ethene is slightly buoyant with $Fr < 0$ and the flow is dominated by convection. The unstable fuel sphere is convected throughout the flask and the distorted volume rapidly mixes by diffusion. The n-hexane and n-dodecane are dominated by buoyancy with $1 \gg Fr > 0$. The initial negative buoyancy results in the fuel spheres settling to the bottom of the flask and then slowly diffusing upward with a stable interface between the fuel-air mixture and air.

The degree of "mixedness" can be studied to quantitatively assess how quickly the fuels mix within the flask. The intensity of segregation can be defined in terms of the coefficient of variation as described in Kukukova, Aubin and Kresta (2009) as:

$$c_\mathrm{v} = \sqrt{\frac{1}{N}\sum_{i=1}^{N}\left(\frac{X_i - \overline{X}}{\overline{X}}\right)^2} \tag{9}$$

where X_i is the fuel mole fraction for a given computation cell, $\overline{X}$ is the volume average fuel mole fraction, and N is the total number of cells in the domain. The coefficient of variation, c_v, can be normalized by the initial $c_\mathrm{v}(0)$ to obtain a value between 0 and 1. Given that c_v computes the standard deviation over the mean, the value is largest for a perfectly unmixed state and will decay to 0 for a completely homogeneous mixture. As c_v is dimensionless, it can be readily compared between the different fuel cases. Figure 10 plots c_v against time for the three fuels. In very early times, the mixedness of n-hexane and n-dodecane decays more rapidly than ethene. This is caused by the strong buoyancy force that immediately drives the heavier fuels to the bottom of the flask. However, as time continues, ethene c_v reaches a steady value near zero significantly faster than for n-hexane and n-dodecane.

Table 3
Molecular weight, Lennard-Jones parameter, fuel sphere density, Schmidt number, and Froude numbers for the three tested fuels

Fuel	W_F [kg· kmol^{-1}]	σ_F [nm]	ρ_F [kg·m^{-3}]	Sc	Fr
C_2H_4	28	0.39	0.65	0.93	-0.27
nC_6H_{14}	86	0.59	2.00	1.8	0.059
$nC_{12}H_{26}$	170	0.76	3.95	2.6	0.053

The effect of diffusivity on mixing can be understood by examining the estimated Schmidt numbers, Sc, in Table 3. The increase in Sc with increasing fuel molecular weight is primarily due to the decrease in diffusivity with increasing fuel molecule size, although there is a small contribution (15%) from the difference in mixture kinematic viscosity. For example, consider how the binary diffusion coefficient

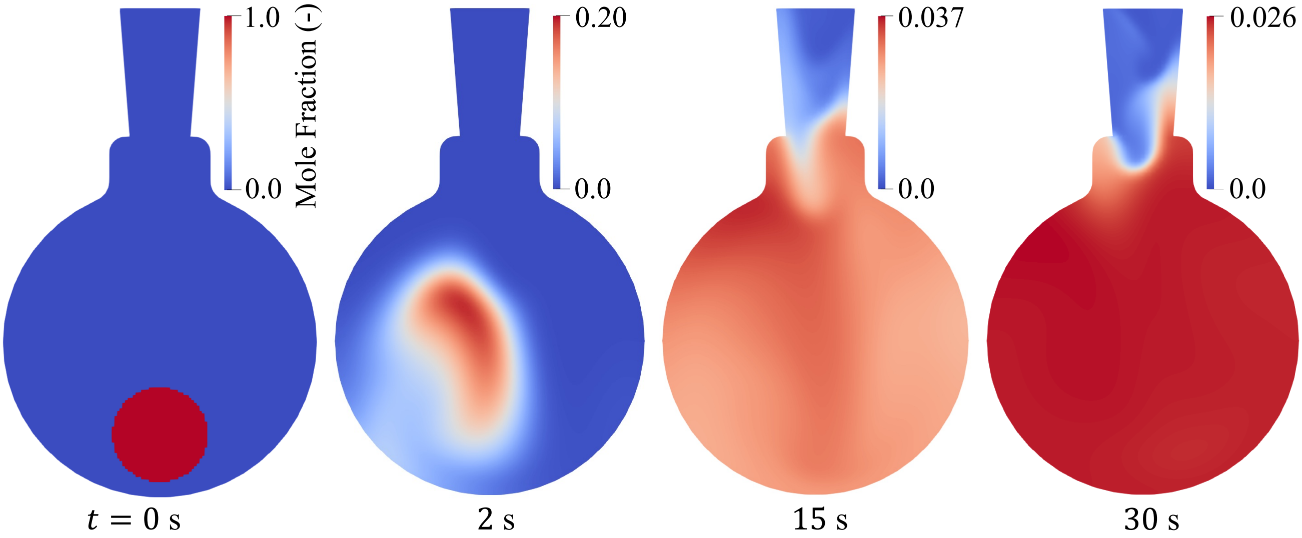

Figure 8: C_2H_4 mole fraction temporal evolution on a vertical cross-section within the flask

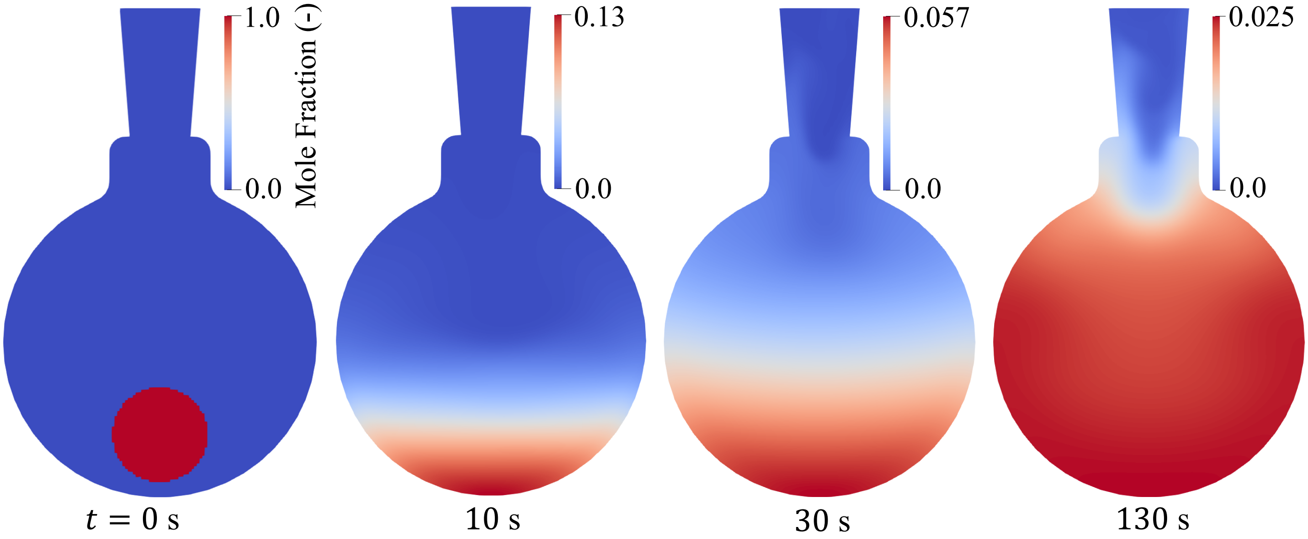

Figure 9: nC_6H_{14} mole fraction temporal evolution on a vertical cross-section within the flask

(Kee, Coltrin and Glarborg, 2005) depends on both the molecular weights W_i and effective collision cross sections σ^2_{FA}

$$D_{FA} \propto \frac{1}{\sigma^2_{FA}} \sqrt{\frac{1}{W_F} + \frac{1}{W_A}}$$

where $\sigma_{FA} = (\sigma_F + \sigma_A)/2$ and $\sigma_A = 0.35$ nm. The increase in molecular size σ_F and decrease in diffusivity for the larger fuel molecules results in an increase in the time to mix, all other factors being the same. This accounts for the differences in the mixing rate of n-hexane and n-dodecane.

Taking a 5% level of c_v conventionally used in industry to characterize mixing time, the time to mix was = 11, 59, and 104 s for C_2H_4, nC_6H_{14}, and $nC_{12}H_{26}$, respectively. Previous work from Martin (2023) shows that nC_6H_{14} and $nC_{12}H_{26}$ can ignite before these times in some ASTM test conditions. In those cases, it is probable that ignition occurs before the fuel is fully mixed inside the flask.

A mixing investigation of C_2H_4 and nC_6H_{14} fuel spheres initialized at room temperature was also carried out. The results are presented in blue in Figure 10. The lower temperature, higher density C_2H_4 sank to the bottom of the flask, similar to what was observed for the heavy hot fuels. The lower temperature, higher density nC_6H_{14} sank to the bottom of the flask with a greater acceleration compared to the flask ambient temperature case. This additional buoyancy induced acceleration seen for both cold fuels resulted in greater mixing during the initial transient (< 10 s). For the faster mixing C_2H_4, this resulted in a reduction in the time to mix from 11 s to 7 s. Later in time for the nC_6H_{14} case (> 20 s), after the initial transient damps, the fuel layer is stably stratified and the subsequent mixing is primarily through molecular diffusion. This resulted in a time to mix that remained at 59 s for both the room temperature and the flask ambient temperature n-hexane fuel case.

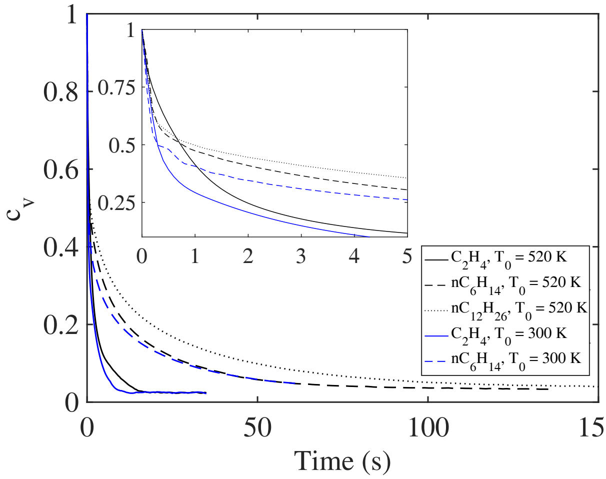

Figure 10: Coefficient of variation (9) over time for C_2H_4, nC_6H_{14}, and $nC_{12}H_{26}$ initialized at flask ambient temperature. Results are also provided for C_2H_4, nC_6H_{14} initialized at room temperature

The number of fuel moles, *n*, within the flask can also be tracked over time by integrating spatially over the number of cells. This is shown in Figure 11. Since the same volume, pressure, and temperature were initialized, *n* is initially the same for all three cases. After 3 seconds, ethene molecules begin leaving the flask and the number of moles rapidly decreases over the next several seconds. After 26 s, 10% of the fuel has escaped into the holder and ambient air above. For n-hexane and n-dodecane cases, a 10% loss of fuel takes significantly longer at 117 and 173 s, respectively. The much slower loss of the larger, heavier fuel molecules is a consequence of the stable stratification, resulting in a much longer time for the fuel-air interface to reach the top of the flask, diffuse into the neck of the flask, and, ultimately, escape. For all cases, the time to lose 10% of the fuel molecules is longer than the time for the intensity of segregation to drop below 5%. Thus, the fuel molecules remain mostly within the flask prior to complete mixing, even for the smaller, lighter C_2H_4 case. Martin (2023) observed ignition of n-hexane and n-dodecane up to approximately 70 and 170 seconds, respectively. It's probable that less than 10% of the fuel leaves the flask before he observed ignition.

The mixing results presented are for a highly idealized fuel initialization. For liquid fuels, such as nC_6H_{14} and $nC_{12}H_{26}$, rapid vaporization of the fuel droplets is expected to create a substantial transient velocity field inside the flask due to the volume displacement of air within the flask. For gaseous fuels, such as C_2H_4, the momentum of the jet of injected fuel will also induce flow and displacement. In both cases, the initial distribution of fuel composition and temperature will be quite different than the idealized spherical ball. Our simulations are intended to guide the understanding of the effects of the initial flow field on the composition at later times characteristic of a long duration autoignition test.

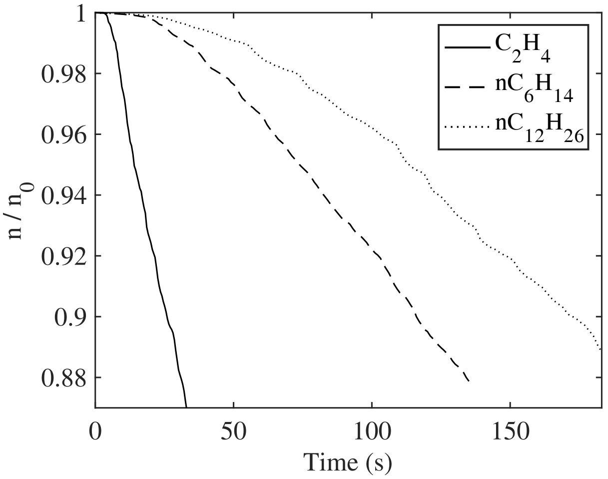

Figure 11: Number of fuel moles normalized by the initial value within the flask over time

5. Implications for AIT experiments

Our results (Figures 4 - 7) indicate that various setups conforming to the ASTM-E659 (2005) standard exhibit a dominant toroidal vortex within the flask, driven by cold plumes of air sinking through the center of the flask from the open top. This effect is a feature of buoyancy driven nonreactive flow and is distinct from the vortical flows produced by exothermic chemical reaction. The vortex rotation direction in a closed spherical vessel undergoing self-heating is the opposite direction and a different order of magnitude (smaller) than that due to the cold air intrusion.

The downward sinking cold air will be a feature of any test apparatus that is open to the surrounding atmosphere at the mouth of the flask. This is the case not only for an ASTM-E659 flask, but also the IEC and DIN apparatus outlined in the ISO/IEC 80079-20-1 (2017) standard which include an open top in a shorter neck and smaller flask volume than the E659 standard. For long duration, up to 600 s, tests used to define the AIT, temperature variations induced by the sinking cold air intruding through the open neck of the flask may be comparable to those due to buoyancy effects associated with to energy release and temperature variations on flask surface.

The temperature and composition fluctuations created by influx and mixing of cold air will influence the self-heating process, an additional source of variability in reported AIT values. The results presented in Figure 7 further indicate that variations in the implementation of the ASTM-E659 standard can have significantly different temperature distributions. A range of temperatures can exist within the flask and will not be captured by the single point of measurement at T_4. Further, the size of fluctuations and general unsteadiness are different for the three cases we considered. This indicates that investigation and consideration of variations between apparatus construction is needed when evaluating reported results. The existence of a range of temperatures within the test flask indicates that care is needed in interpreting the values of AIT based only on the measurements of T_4.

We observe that fuel dispersion inside the flask is affected by the flow field and the fuel's physical properties, such as the density and diffusion coefficient. For short-duration tests, ignition could occur in a poorly mixed, stratified atmosphere, while for long-duration tests, loss of fuel could influence the AIT. Competing mixing and chemical timescales could cause AIT comparisons between different fuels to be misleading unless these factors are taken into account.

6. Conclusions

Experimental measurements and three-dimensional numerical simulations with realistic transport properties were used to characterize the nonreactive flow field inside our ASTM-E659 Autoignition Temperature (AIT) facility. Within the test flask, the downward movement of air through the center of the neck create a single dominant toroidal vortex that transports gas upwards along the walls and downward along the center line. The observed toroidal vortex is counter-rotating and exists in a non-reacting flow compared to results from numerous previous studies in closed spherical vessels. This is a direct consequence of the open flask configuration used in AIT testing in order to visualize emission from the flame.

Temperature measurements were made along the vertical center line in our AIT facility and were compared to a numerical simulation of the same geometry. A maximum variation of 4 K (0.7%) was observed in the average temperature within the flask. Above the flask, larger deviations between the simulation and experiment were observed due to the isothermal boundary condition used on the numerical model. For all measured locations, experimental temperature fluctuations were significantly smaller than those seen in the simulation at the same location, These differences are attributed to the the slow response time of the thermocouple used in the experimental measurements.

A parametric study of the ceramic holder heights was carried out numerically to observe the effect on the resultant flow field. While the same toroidal vortex pattern was seen within the bottom of the flask for all cases, the strength decreased with increasing holder height as the cold plume influx to the flask decreased in these cases. As a result, the average temperature for any given location along the vertical center line increased with increasing holder height. At the center of the flask, the average temperature for case A (shortest) was 7 K lower than for case C (tallest). Similarly, the absolute fluctuation size decreased from 8 K with the shortest holder to 0.9 K for the tallest holder.

A parametric study was also carried out to observe the effect of varying fuel molecule size and molecular weight on the mixing process within the flask. For the smallest molecule, ethene, complete mixing can occur in only 11 s due to minimal buoyancy effects and small Schmidt number. Heavier fuels, such as n-hexane and n-dodecane, consequently have much smaller, positive Froude numbers. Therefore, gravity initially plays a dominant role in forcing the fuel to the bottom of the flask. With significantly larger Schmidt numbers, these fuels diffuse much more slowly in air with mixing times of 59 and 104 s respectively, compared to ethene. A 10% loss of fuel molecules was observed after 25, 119, and 180 s for ethene, n-hexane, and n-dodecane, respectively. Therefore for all fuels studied, significant loss of fuel from the flask only occurs after complete mixing is obtained. The mixing character for ethene was found to be affected by the initial fuel temperature whereas for n-hexane, the time to mix was unchanged with a changing initial fuel temperature.

Our study has identified a number of factors that are important to consider in interpreting AIT data from the ASTM-E659 apparatus. We observe that both the construction of the apparatus (with the allowable specification of the standard) and the fluid motion induced by buoyancy through the open top can have a significant influence of gas inside the flask prior to fuel injection as well as chemical reaction progress after injection. The observed variability in temperature and fuel concentration may have an influence on the measured autoignition temperatures and ignition delay times with implications for application to hazard assessment.

Acknowledgements

This research was carried out in the Explosion Dynamics Laboratory of the California Institute of Technology. This work was supported by The Boeing Company through a Strategic Research and Development Relationship Agreement CT-BA-GTA-1 and C. Fouchier was supported by the HORIZON-MMSCA-2021 Postdoctoral Fellowship Program, Project #101063624.

References

Ashmore, P., Tyler, B., Wesley, T., 1967. Experimental investigations of conductive and convective heat transfer in relation to thermal ignitions, in: Symposium (International) on Combustion, Elsevier. pp. 1133–1140.

ASTM-E659, 2005. Standard test method for autoignition temperature of liquid chemicals. American Society for Testing and Materials.

Babrauskas, V., 2003. Ignition Handbook. Fire Sciences Publishers, Society of Fire Protection Engineers.

Bowes, P., 1984. Self-heating: evaluating and controlling the hazards. Department of the Environment, Building Research Establishment .

Campbell, A., Cardoso, S., Hayhurst, A., 2007. A comparison of measured temperatures with those calculated numerically and analytically for an exothermic chemical reaction inside a spherical batch reactor with natural convection. Chemical Engineering Science 62, 3068–3082.

Chapman, S., Cowling, T.G., 1990. The mathematical theory of non-uniform gases: an account of the kinetic theory of viscosity, thermal conduction and diffusion in gases. Cambridge university press.

Coffee, T., Heimerl, J., 1981. Transport algorithms for premixed, laminar steady-state flames. Combust. Flame 43, 273–289.

Curtiss, C.F., Hirschfelder, J.O., 1949. Transport properties of multicomponent gas mixtures. J. Chem. Phys. 17, 550–555.

Frank-Kamenetskii, D., 1939. Calculation of thermal explosion limits. Acta Physicochemica U.R.S.S 10, 365–370.

Hattwig, M., Steen, H. (Eds.), 2004. Handbook of Explosion Prevention and Protection. Wiley-VCH Verlag GmbH & Co. KGaA, Weinheim, FRG.

Iglesias, I., Moreno-Boza, D., Sánchez, A., Liñán, A., Williams, F., 2017. Thermal explosions in spherical vessels at large Rayleigh numbers. International Journal of Heat and Mass Transfer 115, 1042–1053.

ISO/IEC 80079-20-1, 2017. ISO/IEC 80079-20-1: Explosive Atmospheres - Part 20-1: Material Characteristics for Gas and Vapor Classification-Test Methods and Data. Technical Report. International Organization for Standardization.

Johnson, C., Mashuga, C.V., 2023. Reconsidering autoignition in the context of modern process safety: Literature review and experimental analysis. Journal of Loss Prevention in the Process Industries 81, 104963.

Jones, D., 1974. Convective effects in enclosed, exothermically reacting gases. International Journal of Heat and Mass Transfer 17, 11–21.

Kee, R.J., Coltrin, M.E., Glarborg, P., 2005. Chemically reacting flow: theory and practice. John Wiley & Sons.

Kee, R.J., Landram, C.S., Miles, J.C., 1975. Natural Convection of a Heat-Generating Fluid Within Closed Vertical Cylinders and Spheres. Technical Report SAND75-8610. Sandia Laboratories. Livermore CA.

Kukukova, A., Aubin, J., Kresta, S.M., 2009. A new definition of mixing and segregation: Three dimensions of a key process variable. Chemical engineering research and design 87, 633–647.

Liñán, A., Moreno-Boza, D., Iglesias, I., Sánchez, A.L., Williams, F.A., 2016. The slowly reacting mode of combustion of gaseous mixtures in spherical vessels. Part 1: Transient analysis and explosion limits. Combustion Theory and Modelling 20, 1010–1028.

Liu, T.Y., Campbell, A.N., Hayhurst, A.N., Cardoso, S.S., 2010. On the occurrence of thermal explosion in a reacting gas: The effects of natural convection and consumption of reactant. Combustion and Flame 157, 230–239.

Lüth, P., Brandes, E., Stolz, T., 2014. Interlaboratory Test 2012 - 2013 on the Method EN 14522:2005 "Determination of the Auto Ignition Temperature of Gases and Vapours" - IEC 60079-20-1, Part 7 "Method of Test for Autoignition Temperature: Final Report. BAM, Bundesforschungsanstalt für Materialforschung und -prüfung, Berlin.

Martin, C.D., 2023. Experiments in Thermal Ignition: Influence of Natural Convection on Properties of Gaseous Explosions. Ph.D. thesis. California Institute of Technology.

Martin, C.D., Shepherd, J.E., 2021. Low temperature autoignition of Jet A and surrogate jet fuel. Journal of Loss Prevention in the Process Industries 71, 104454.

Melguizo-Gavilanes, J., Boettcher, P., Mével, R., Shepherd, J., 2019. Numerical study of the transition between slow reaction and ignition in a cylindrical vessel. Combustion and Flame 204, 116–136.

Rice, O., Allen, A.O., Campbell, H.C., 1935. The induction period in gaseous thermal explosions1. Journal of the American Chemical Society 57, 2212–2222.

Rice, O., Campbell, H.C., 1939. The explosion of ethyl azide in the presence of diethyl ether. The Journal of Chemical Physics 7, 700–709.

Sánchez, A.L., Iglesias, I., Moreno-Boza, D., Liñán, A., Williams, F.A., 2016. The slowly reacting mode of combustion of gaseous mixtures in spherical vessels. Part 2: Buoyancy-induced motion and its effect on the explosion limits. Combustion Theory and Modelling 20, 1029–1045.

Semenov, N., 1928. Zur theorie des verbrennungsprozesses. Zeitschrift für Physik 48, 571–582.

Setchkin, N.P., 1954. Self-ignition temperatures of combustible liquids. Journal of Research of the National Bureau of Standards 53, 49.

Silakova, M., Smetanyuk, V., Pasman, H., 2006. Model, software for calculation of ait and its validation. URL: `https://www.morechemistry.com/SAFEKINEX/`. Deliverable No. 18 of SAFEKINEX:SAFe and Efficient hydrocarbon oxidation processes by KINetics and Explosion eXpertise.

The Open Foam Foundation, 2023. OpenFOAM. `https://www.openfoam.org/`.

Tyler, B., 1966. An experimental investigation of conductive and convective heat transfer during exothermic gas phase reactions. Combustion and Flame 10, 90–91.

Tyler, B., Tuck, A., 1967. Heat transfer to a gas from a spherical enclosure: Measurements and mechanism. International Journal of Heat and Mass Transfer 10, 251–253.

USCG, 1999. Chemical hazard response information system (CHRIS)-hazardous chemical data. Technical Report Commandant Instruction No. 16465. United States Coast Guard.

Zabetakis, M.G., Furno, A.L., Jones, G.W., 1954. Minimum spontaneous ignition temperatures of combustibles in air. Industrial & Engineering Chemistry 46, 2173–2178.

Zakel, S., Brandes, E., Schröder, V., 2019. Reliable safety characteristics of flammable gases and liquids–the database chemsafe. Journal of Loss Prevention in the Process Industries 62, 103914.

Zeldovich, Ya.B., Barenblatt, G.I., Librovich, V.B., Makhviladze, G.M., 1985. The Mathematical Theory of Combustion and Explosions. Consultants Bureau.